Title: **Interaction force between magnetic field and ferromagnetic target: analytical, numerical and experimental study**

Authors: **P. Neri**

DOI Link: https://doi.org/10.1177/0037549718782398

Interaction force between magnetic field and ferromagnetic target: analytical, numerical and experimental study

Journal Title
XX(X):1–9

DOI: 10.1177/ToBeAssigned
www.sagepub.com/
SAGE

Paolo Neri[1]

Abstract

In this paper, an analytical model and a Finite Element model are developed in order to study the force produced by a permanent magnet on a ferromagnetic target. The study is aimed at estimating the magnetic action in order to design an excitation device for vibration tests. The dynamic analysis of rotating structures as compressors' bladed wheels requires a solicitation which reflects the operational conditions. If the component is made of ferromagnetic material, it is possible to use magnetic fields for the excitation. In the present paper, the interaction between planar parallel surfaces was firstly analytically and numerically studied, and the results were compared with experimental results. Then the interaction between sloping surfaces was analysed, allowing to develop an analytical boundary loss model. Finally, the FE model was improved to study the interaction between double curvature surfaces. A comparison with experimental results measured on an actual bladed wheel was performed.

Keywords

Permanent magnet model, Magnetic force model, Boundary loss model, Bladed wheels excitation

Introduction

Rotating components dynamic analysis is a crucial issue in many industry fields, where the optimization process along with the performance enhancement let the machine parts operate in really severe working conditions. Centrifugal compressors and turbines bladed wheels surely represent a good example of this issue, experiencing a cyclic load due to the interaction with the fluid coming from the stator vanes. This loading can generate a vibrational response of the components, thus leading to noise, efficiency loss, fretting and blades fatigue failures.

Resonance prediction is a crucial issue from design stage to validation stage, in order to avoid resonance conditions and to reduce costly maintenance plant shut down [1–4]. Two main criteria are available in literature for bladed wheels: the Campbell diagram [5] and the Singh's Advanced Frequency Evaluation (SAFE) diagram [6–8]. In particular, the SAFE diagram showed to provide the more reliable results [9–12] for bladed wheels resonance prediction. Anyway, both the methods rely on a deep knowledge of the dynamic behaviour of the wheels. Geometrical details, boundary conditions and machining errors can influence the dynamic response of the machine and are not easily considered by Finite Element (FE) analysis, so that the experimental approach is really important. Moreover, the SAFE diagram criterion highlights that a full resonance should be expected in bladed wheels when two conditions are fulfilled: load and natural mode frequency matching and load spatial distribution and modal shape matching. This latter condition implies that a specific spatial distribution of the load is needed to properly excite a particular mode. A proper estimation of the time varying force acting on each blade is then crucial when designing a test, especially if operational conditions need to be simulated. If the bladed wheel is manufactured using ferromagnetic materials, the solicitation can be introduced by magnetic fields. Electromagnets represents a really flexible contact-less solution, allowing to reproduce the desired spatial and temporal force distribution by acting on the electronic control of the device [13–17]. A preliminary step in the design of such excitation device is represented by the estimation of the interaction force between the magnetic field and the ferromagnetic target. A really simple approach is to consider permanent magnets as a magnetic field source, in order to perform really simple tests to study the phenomenon. Permanent magnets have also been directly used as en excitation source for dynamic tests [18]. Anyway, since the magnetic field produced by the magnet is constant, the only way to produce a varying force on the component would be to actuate the wheel (or the magnets set) with a rotating motor. This would cause safety issues and would also require an expensive equipment, since a high power would be needed to reach the typical working rotational speed (more then 10000 rpm). This is the reason why the present work is not aimed at designing a permanent magnet exciter, but it represents a preliminary study on the force produced by a magnetic field on a ferromagnetic target. Two different models were then developed to study this interaction: a numerical (FE) model and an analytical model. The first model allowed to simulate general test conditions, even if pretty long computation time was needed. Several papers are available in literature for magnetic field finite element analysis [19–24].

[1]Department of Civil and Industrial Engineering, University of Pisa, Largo Lucio Lazzarino, Pisa, 56122, Italy

Corresponding author:
Paolo Neri, Department of Civil and Industrial Engineering, University of Pisa, Largo Lucio Lazzarino, Pisa 56122, Italy.
Email: paolo.neri@dici.unipi.it

The second model was less accurate and less flexible but could estimate in a really short time the effect of the different design parameters. Several examples of this kind of model are available in literature in different fields[25,26].

This paper presents the main hypothesis used in the proposed models; the obtained results are also compared with experimental data. The focus was firstly set on simplified cases, where the interaction of the magnet and the target happens through planar parallel surfaces. A simple experimental test allowed to validate a 2D FE model. This model was then used to simulate sloping plane surfaces, in order to have reference values to compare with the analytical model results, without the need to perform more complex experiments. Finally, the FE model was extended to the case of double-curvature surfaces. This more complex 3D model was validated by comparing its result with experimental data obtained on a centrifugal compressor bladed wheel.

Materials and methods

Experimental tests

The experimental tests were crucial to validate numerical and analytical models. The aim of the models was to estimate the force acting between the permanent magnets and the ferromagnetic target. This force strongly depends on the geometry of the air gap between the magnets and the target. The test were performed by placing the magnets at a known distance from the target. The distance was then decreased step by step while the force was measured by a load cell. To achieve this testing conditions both the magnet and the target were mounted on the grasping system of an MTS machine for tensile tests. This allowed to precisely change the gap size with a precision of 0.1 mm while measuring the force with a 10 kN load cell (having a precision of 0.5 N). The first test was performed with both target and magnet having planar parallel surfaces. A rectangular Nd-Fe-B permanent magnet was used ($20 \times 100 \times 5$ mm), having a magnetization of 1.15 T. The magnet was inserted in a slot drilled on an iron support. The rectangular iron target was designed to be bigger than the magnet support, in order to reduce the misalignment effects (i.e. a possible $\Delta\vartheta$ between the magnet and the target). A schematic view of the the test set-up is reported in Fig.1. The test was performed for values of l varying from 15 mm to 0.1 mm, and it was repeated twice: firstly with decreasing values of l and then with increasing values of l for comparison purpose.

A more complex test was then performed. A set of permanent magnets was faced to the rotor of a centrifugal compressor, measuring the interaction force. In this situation the surface of the target (i.e. the 15 blades of the rotor) was highly three-dimensional, so that the average distance between the target and the magnets was much higher than the one achieved with the previews test set-up. A lower interaction force was expected, losing measurement accuracy due to the load cell performance. In order to reduce this problem, a support was designed to hold one magnet for each blade, in order to load all the rotor's blades simultaneously, increasing the total force. Cylindrical Nd-Fe-B permanent magnets were chosen for the test, having a 30 mm diameter, a 15 mm height and a magnetization of 1.3 T. The magnets were held in slots drilled in a cylindrical ferromagnetic

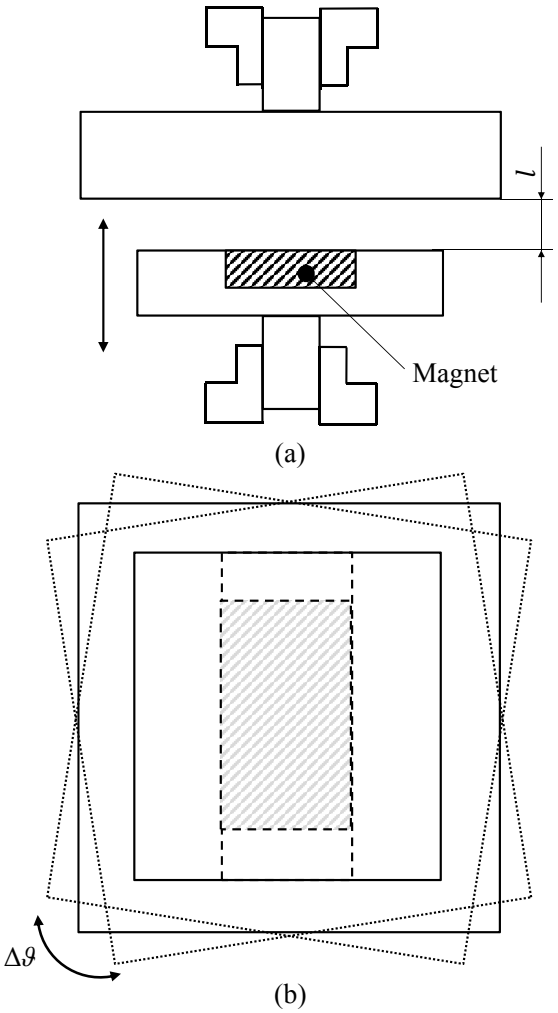

Figure 1. Test set-up scheme: (a) section view; (b) bottom view.

support. An iron piston could move inside the support, having the same diameter of the magnet, for mounting and dismounting purposes, Fig.2(a). All the magnet supports were then mounted on an aluminum disk with fifteen radial slots. This allowed to perform tests with different radial positions of the magnets. The complete disk was then screwed to the load cell and mounted on the upper grasp of the test machine. The bladed wheel was mounted on the lower grasp of the machine instead, Fig.2(b). The aim of the test was to measure the interaction force corresponding to different air gaps between magnets and target (for FE model validation). Since the absolute measure of the air gap was not known because of its shape, the test zero-distance was set using a cylindrical spacer, using the rotor shaft and the support-disk surface as references. This allowed to find an axial zero-position which was known in the test and in the FE model. The upper grasp was then lowered during the test, reducing the air gap (thus obtaining negative displacements). Since no angular references were physically available on the rotor, the zero-angular position was determined by placing the magnets at a known distance from the rotor. The lower grasp was then rotated (0.5^{o} steps) in order to find the maximum of the force. It was then possible to align numerical and experimental results by repeating the same procedure in the FE model and by looking for the angle which gave the maximum force in both cases.

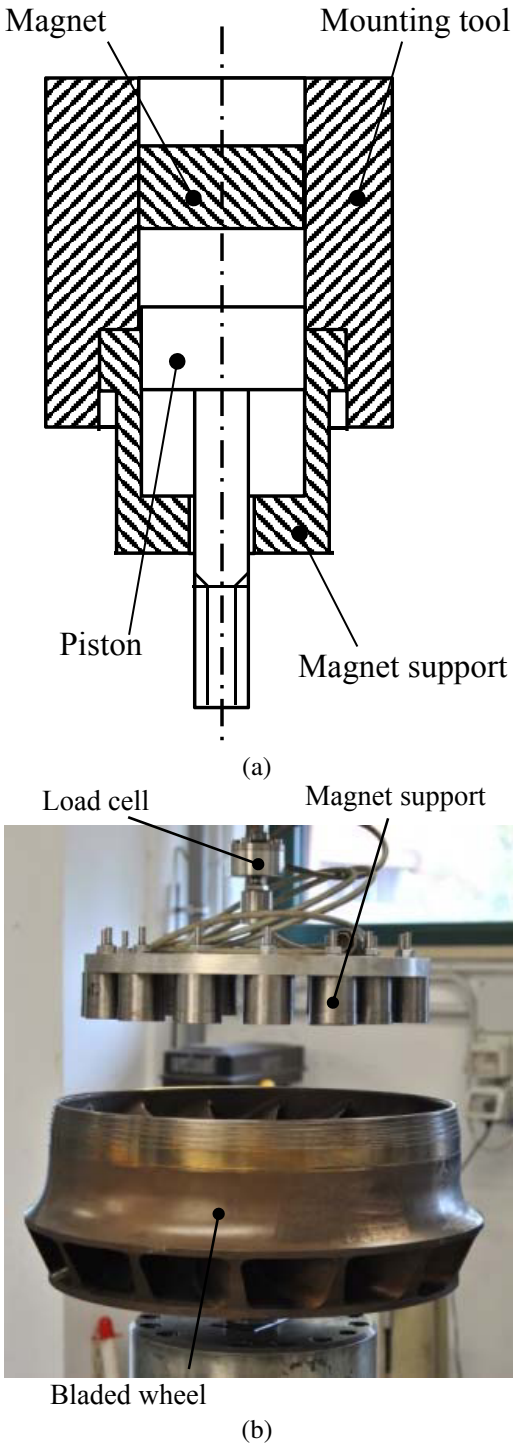

Figure 2. Test set-up: (a) magnet support scheme; (b) set-up view.

The first test was performed with a fixed axial distance (-39 mm, considering the same axial zero used to plot Fig.13(b)), varying the angular positioning. The test was then repeated with a fixed angular position (corresponding to the maximum force), varying the axial distance. In both cases, the test was repeated twice in the two directions, to check the proper execution of the test.

FE model

A FE model was developed using the software "Maxwell". The configuration with planar parallel surfaces was firstly simulated. A 2D model was set-up to reduce simulation time. Fig.3(a) shows the mesh used for the magnet, its support, the target and the surrounding air region, while Fig.3(b) shows the flux lines corresponding to $l = 4.0$ mm.

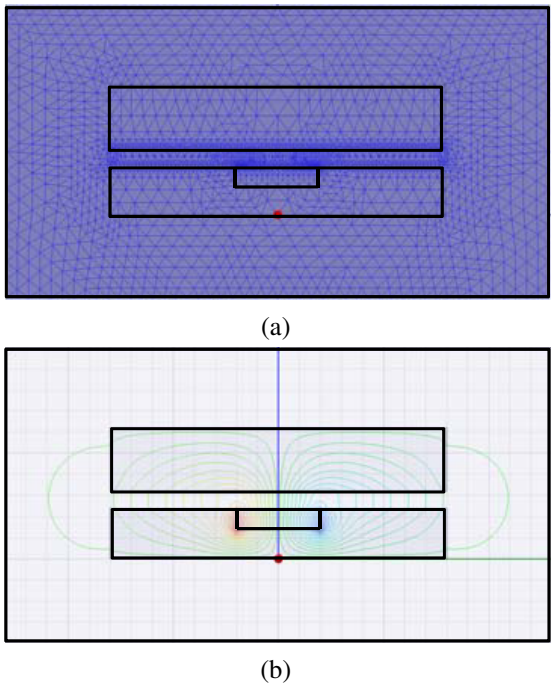

Figure 3. FE model: (a) mesh; (b) flux lines for $l = 4$ mm.

The FE model was able to compute the line force acting on the target for unit length (N/m), so that it was possible to obtain the actual value to compare with experimental and analytical results by multiplying FE data by the actual length of the considered magnet. The 2D model was then used to perform parametric analysis, varying the magnet width or changing the angle between the magnet support and the target. This allowed to simulate several magnet-target interactions without performing experimental tests, having a simulation time shorter than the one expected with a 3D model. Those results were used to validate the force estimation obtained with the developed analytical model (see below).

Finally, a 3D FE model was developed to study the effects of a target with double curvature surfaces, in order to simulate the interaction between permanent magnets and blades, Fig.4(a). Cyclic symmetry conditions were imposed in order to reduce the number of elements. Only one wheel sector was modeled, having an angular extension of $360^{\circ}/N_{\mathrm{B}} = 24^{\circ}$. This allowed to simulate a test configuration with 15 magnets faced to the 15 blades of the wheel by only considering one sector. To achieve this result, a "Master" surface was defined on one face of the sector and a "Slave" surface was defined on the other, imposing the equality of the magnetic field on these two faces to respect cyclic symmetry conditions, Fig.4(b). Parametric analyses could be executed in order to simulate different configurations in terms of axial distance between magnets and blades and different radial or angular positioning of the excitation source with respect to the target.

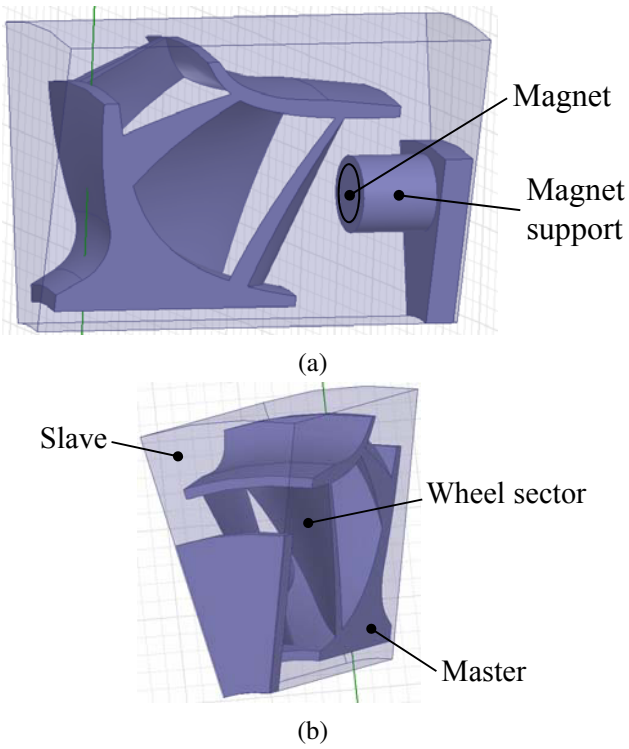

Figure 4. Wheel sector 3D FE model: (a) geometry; (b) boundary conditions.

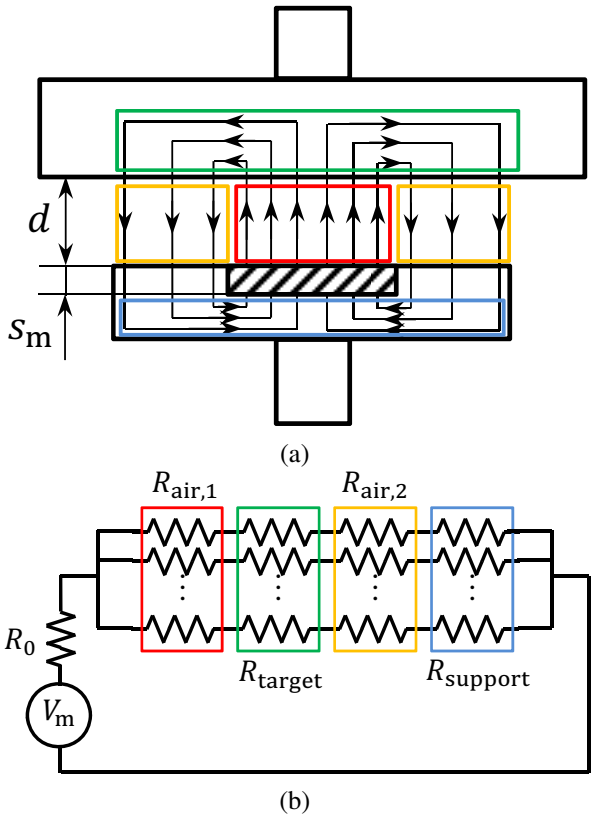

Figure 5. Model scheme: (a) flux lines; (b) equivalent circuit.

Analytical model

An analytical model was developed basing on the equivalent circuit method[27]. The permanent magnet was represented as a tension generator with an in-series resistor (R_0), while the magnet support, the target and the air gap were schematized as a circuit of parallel or in-series resistors (Fig.5(b)).

The resistence R of each resistor was evaluated using the equation:

$$R = \frac{l}{\mu A} \tag{1}$$

where l and A represent the length and the cross section of the considered object (respectively), while μ represents the permeability of the material. The equivalent properties of the permanent magnet can be computed using the equation[27]:

$$R_0 = \frac{s_m}{\mu_m A_m} \tag{2}$$

$$v_m = H_c s_m \tag{3}$$

where A_m is the area of the magnet facing the target, s_m is the magnet thickness, μ_m is its magnetic permeability and H_c is the coercive force ($H_c = B_r/\mu_m$). In order to exactly compute the value of the equivalent resistor of the circuit, a precise knowledge of the flux lines would be needed, so that it could be possible to split the flux lines into known paths whose equivalent resistance could be computed using Eq.1, Fig.5(a). The passage of the flux through sections of different materials is represented in Fig.5(b) with the in-series resistors. Since it is not possible in general to exactly know the path of the flux lines (especially in more complex problems), it was not possible to draw the exact scheme of the equivalent circuit. This is the reason why a simplification was introduced, neglecting the contribution of all the ferromagnetic materials to the equivalent resistance of the circuit. This values indeed is several order of magnitude lower then the resistance of the air gap because of the magnetic permeability values. This implies that all the points of the ferromagnetic material (magnet support and target) share the same potential, representing a node in the equivalent circuit scheme, Fig.6.

This simplification allowed to compute the parallel resistor contained in red and orange rectangles in Fig.6. If the infinitesimal surface dA is considered, its resistance dR can be computed as $\mathrm{d}R = l/\mu \mathrm{d}A$. Using the well known formula for parallel resistors computation, the parallel of the resistors reported in Fig.6(b) can be indicated as $R_{//}$ and computed as:

$$\frac{1}{R_{//}} = \int_{s_{m,s}} \frac{1}{\mathrm{d}R} = \int_{A_{m,s}} \frac{\mu}{l} \mathrm{d}A = \frac{\mu A_{m,s}}{l} \tag{4}$$

where $A_{m,s}$ represents the surface of the magnet (m) or the surface of the support (s) when the different resistors are computed (i.e. $R_{air,1}$ and $R_{air,2}$). Another hypothesis is introduced, considering that all the flux lines are perpendicular to the target surface, so that l in Eq.4 corresponds to the air gap length (i.e. d in Fig.5(a)). Since the air gap is constant in the considered problem, the integral could be solved as reported in Eq.4. It was then possible to compute the value of the magnetic flux by solving the equivalent circuit:

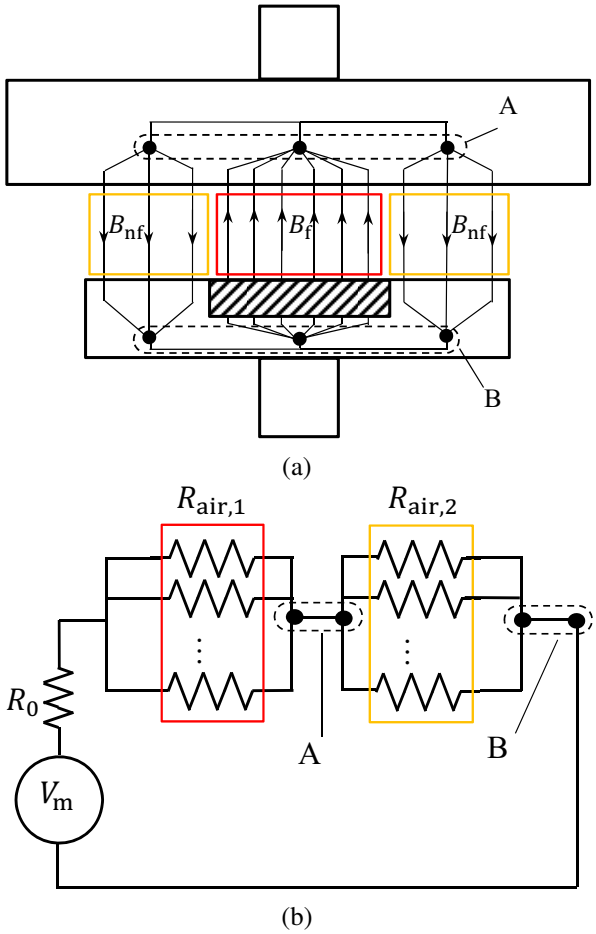

Figure 6. Simplified model scheme: (a) flux lines; (b) equivalent circuit.

$$\phi_g = \frac{V_m}{R_g} = \frac{H_c s_m}{R_{air,1} + R_{air,2} + R_0} \tag{5}$$

where ϕ_g represents the total magnetic flux in the air gap while R_g is the total resistance of the circuit, i.e. the series of the three resistors $R_{air,1}$, $R_{air,2}$ and R_0. It was then possible to compute the interaction force by using the equations:

$$B_f = \phi_g / A_m \tag{6}$$

$$B_{nf} = \phi_g / A_{nf} \tag{7}$$

$$F = 1/2\mu_0 (B_f^2 A_m + B_{nf}^2 A_{nf}) \tag{8}$$

where B_f and B_{nf} represent the magnetic flux density in the air gap facing the permanent magnet and not-facing the permanent magnet respectively, Fig.6(a), while A_m and A_{nf} represent the corresponding areas. Since the FE model showed the presence of boundary losses at the magnet edges (see Fig.10), the analytical model was further developed to also consider this effect. This effects could be introduced in the model by removing from the calculus a portion of the magnet and of the support area, i.e. reducing the value of A_m and A_{nf}. Fig.7 shows the proposed boundary-loss models. The width of the magnet portion to be neglected is indicated with $\bar{s}$, representing the distance between the magnet edge and the last flux line which does not cross the target during its path. The flux line starting at a distance s from the magnet edge will follow the lowest resistance path, i.e. the shorter path available. The round trip path in the complete air gap would have a length of $2d$. The path marked with a red line in Fig.7 has a length $\bar{L}$ instead, which depends on the chosen model and on the distance $\bar{s}$. When the condition $2d = \bar{L}$ is crossed increasing the value of s, the flux lines switch from a path which does not cross the target to a path which crosses the target instead, so that the value of $\bar{s}$ can be found. This allowed to remove from A_m and A_{nf} the portion of material corresponding to $\bar{s}$. These two loss models were then implemented in the script, so that the improved model could be tested in several conditions, varying magnet dimensions and air gap length. This allowed to chose the left side loss model in Fig.7 as the more reliable one.

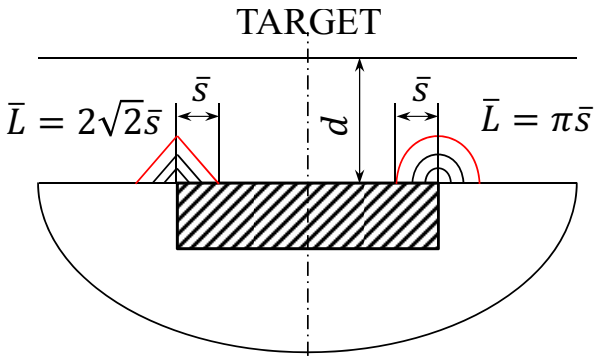

Figure 7. Proposed boundary-loss model.

Finally, the analytical model was further developed by considering the interaction between sloping surfaces, Fig.8. This scenario would allow again to obtain an analytical expression of the equivalent resistance of the circuit by solving the integral of Eq.4. Anyway, future development could lead to a further extension of the model to double-curvature surfaces, whose analytical expression could be unknown. This is the reason why a different approach was followed. The magnet support surface and the target surface were divided into small segments. For each segment, it was possible to compute an equivalent resistor. Finally, the total equivalent resistor can be computed by using the classic formula. Once the equivalent resistor was computed, it was possible to apply the same analytical model described above. Anyway, in this situation the proposed boundary-loss model was not suitable anymore, since the air gap changes size in each location. A different approach was then followed. The path of the flux lines of a permanent magnet in air can be found by using an analytical formula[27]:

$$A = f(x, y, h, w) \tag{9}$$

being x and y the coordinates on the plane, h the magnet height and w the magnet width. Obviously, the presence of the ferromagnetic components influences the actual flux lines path. Anyway, this formula was used just to obtain an estimation of the active part of the magnet, in order to know which amount of the area was to be considered in the force computation, so that the approximation was considered acceptable. A point of the target (x_0, y_0) was considered and the value of $\bar{A}$ corresponding to the flux line passing from that

point was found, Fig.8. A Newton-Raphson method was then used to find the coordinates of the intersection $(\bar{x}, \bar{y})$ between this flux line and the magnet surface $(-w/2 < \bar{x} < w/2, \bar{y} = h/2)$.

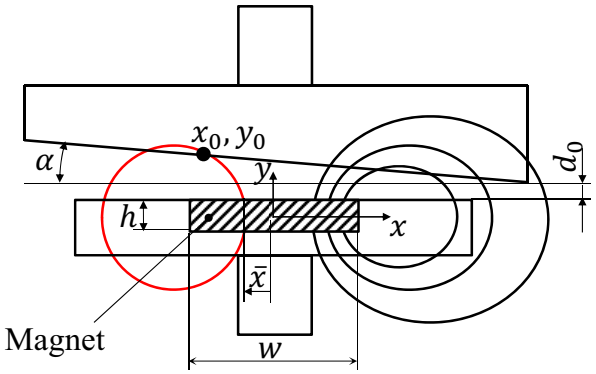

Figure 8. Sloping surfaces schematic view.

It was then possible to obtain a vector containing the values $\bar{x}$ of the points of the magnet which produce a flux line which crosses the target boundary. By looking at the maximum and minimum values of this vector, it was possible to find the edge of the active portion of the magnet in order to compute the proper active area to be used in Eq.6.

Results and discussion

Planar parallel surfaces

The numerical and analytical models developed to simulate the interaction force between planar parallel surfaces were compared with the corresponding experimental results. Figure 9(a) shows the comparison between the experimental test and the FE model. The comparison is really good, except at the lower air gap dimension where the gradient is really high and the 2D model (red dashed line) overestimate the actual experimental force by 14% (corresponding to an absolute error of 84 N). This error was due to the fact that a 2D FE model was considered, neglecting boundary effects and leading to a force overestimation. This statement was confirmed by performing a 3D analysis using the model shown in Fig.9(b). The results of this second model are shown in Fig.9(a) with a black dashed line, reporting a maximum error of 3% with respect to the experimental test (corresponding to an absolute error of 21 N). This comparison allowed to validate the FE model and to ensure that the 2D model gave a good estimation of the force at least for $l > 0.5$ mm.

Once the 2D FE model was validated, it was used to simulate several different geometrical configurations and to compare the results with the analytical model. A preliminary analysis of FE results showed that some boundary-loss happens at magnet edges, since a portion of the magnetic flux follows a path which does not meet the target, Fig.10. Thus, the simplified model (neglecting the boundary-loss) overestimates the traction force acting on the target. This was expected since the model assumes that all the magnetic flux coming from the permanent magnet interacts with the ferromagnetic target.

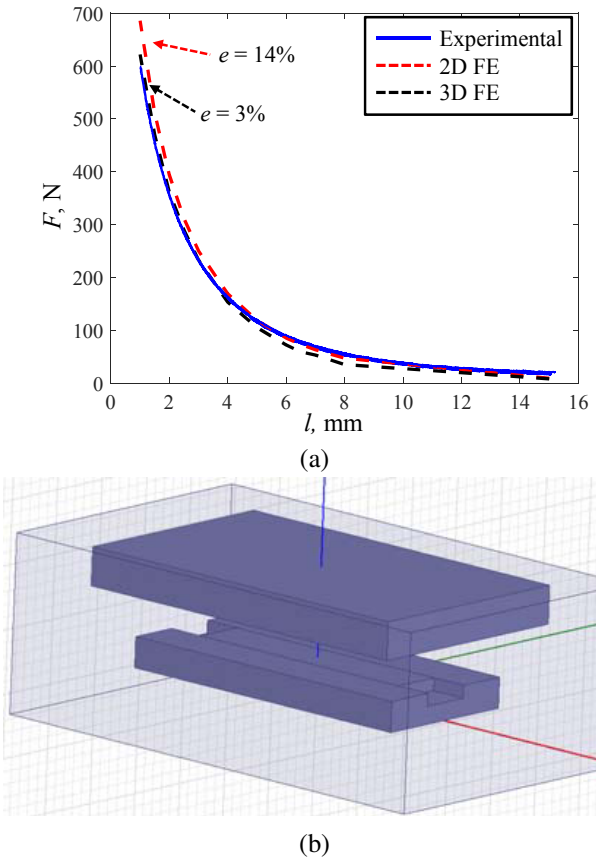

Figure 9. FE analysis: (a) results comparison; (b) 3D model geometry.

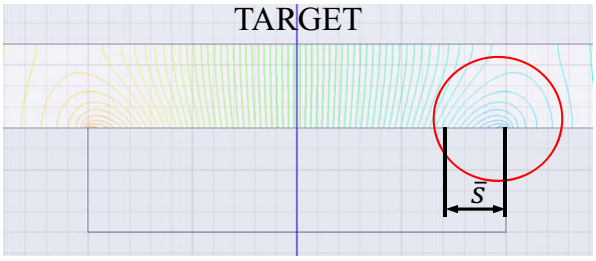

Figure 10. Boundary-loss detected through the FE model

Following these considerations, the boundary-loss model schematized in Fig.7 was implemented. The comparison between numerical and analytical results (considering boundary-loss) corresponding to two different magnet widths are reported in Fig.11. The force provided by the analytical model still overestimates the force computed by the FE model, since the analytical simplified model neglects the resistance of the ferromagnetic material, considers parallel flux lines and neglects boundary effect at the support edges (while the boundary effect at the magnet edges are taken into account). Anyway the results reported in Fig.11 show a good correlation between the analytical and the numerical model for two different magnet width ($w = 20$ mm, Fig.11(a), and $w = 40$ mm, Fig.11(b)), with a relative error lower than 15% in the region of highest gradient.

Planar sloping surfaces

The 2D FE model was used again to validate the results of the analytical model in the case of planar sloping surfaces,

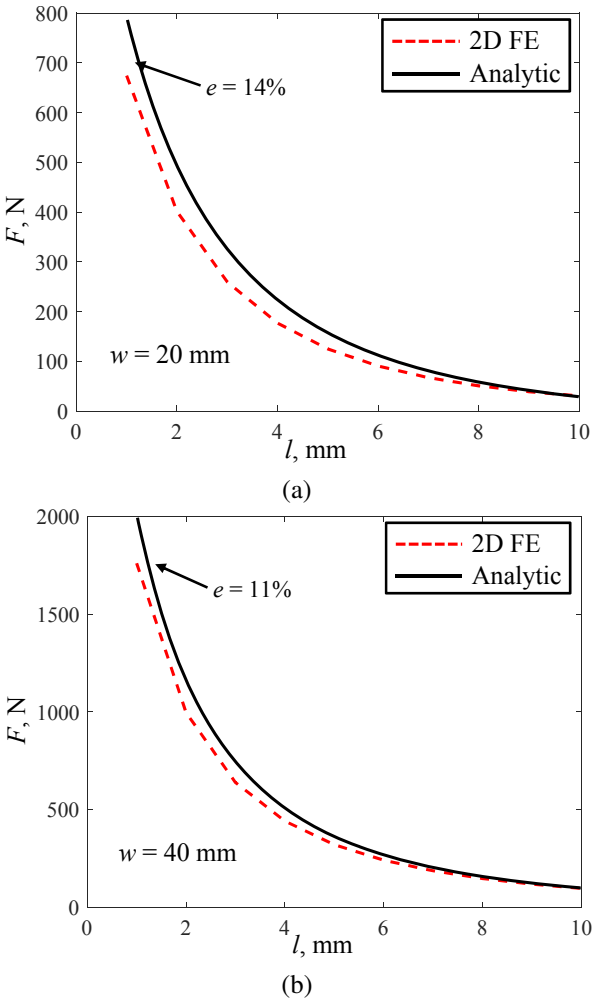

Figure 11. Plane surfaces: comparison between numerical and analytical results.

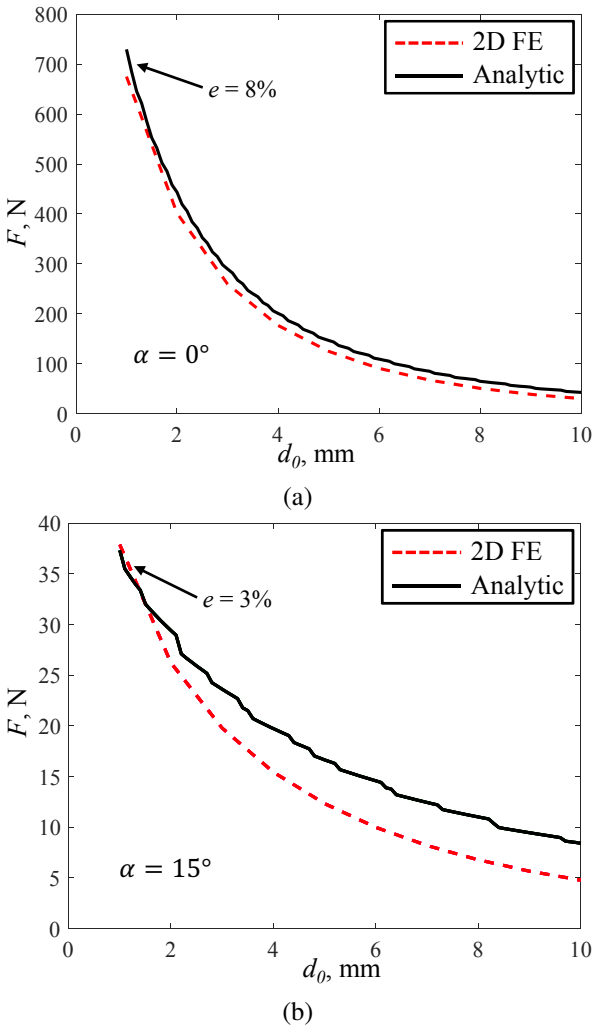

Figure 12. Sloping surfaces: comparison between numerical and analytical results.

Fig.12. This analytical model allows to consider the presence of a varying air gap between the magnet and the target, and also implement a different boundary-loss model for the magnet edges, as explained above. Several combinations of slope angle and magnet dimensions were simulated by exploiting both FE and analytical models. It was possible to simulate again the case of parallel surfaces by setting $\alpha = 0^{o}$. This allowed to asses the performances of the improved boundary-loss model: Fig.12(a) reports the results for this case, showing a maximum error of 8% (i.e. a reduction with respect to the error reported in Fig.11(a)). Moreover, the results corresponding to an angle $\alpha = 15^{o}$ were reported in Fig.12(b). It is worth noting that by increasing the slope of the target and the air gap dimension, the estimation error increases since the boundary-loss becomes more relevant and the proposed estimation model reliability decreases.

Double-curvature surfaces

Finally, the comparison between experimental and numerical data in the case of double-curvature surfaces was performed, Fig.13. Figure 13(a) shows the results obtained for a fixed axial distance and a varying angular position. The black dashed line represents the FE results, while the red and blue lines represent experimental results for a clockwise and a counter-clockwise rotation respectively. Fig.13(b) shows the results obtained for a fixed angular position (corresponding to the maximum force, reported with a dotted vertical line in Fig.13(a)) with a varying axial distance. The black dashed line represents the FE results, while the red and blue lines represent experimental results for decreasing and increasing values of l respectively. As can be seen, the maximum difference between numerical and experimental results is about 20% for the smaller air gap. Since the curve slope is really high for small values of l, experimental results are highly sensitive to small positioning error which may be due to the machining tolerances. It is possible to consider the presence of a 0.5 mm error during the test by shifting the corresponding curve: the black continuous line in Fig.13(b) was then obtained, having a maximum error of about 6% with respect to experimental results.

Conclusions

The presented activity was aimed at estimating the interaction force between permanent magnets and ferromagnetic targets. Experimental tests were used to validate the proposed FE models. An analytical model was also developed to study the interaction force with a shorter computational time than the one required by FE models, with a good approximation level. The comparison with experimental and

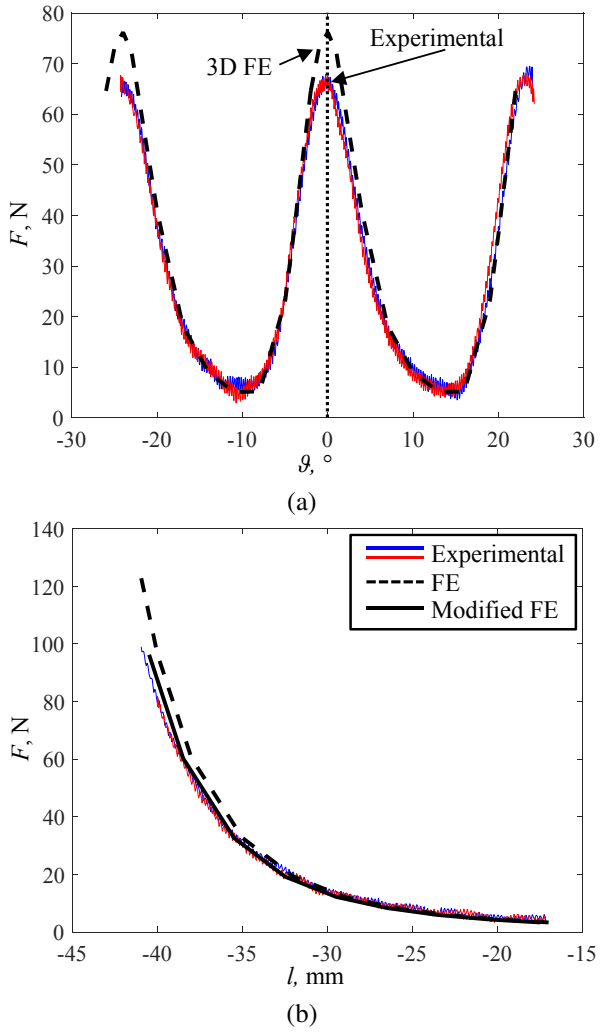

Figure 13. Results comparison: (a) rotational test; (b) axial test.

numerical results allowed to develop an analytical boundary loss model. Further development could allow to extend the analytical model in a semi-analytic fashion to the case of generic surfaces, whose analytical expression is not available. An improved 3D boundary-loss model could also be studied to further extend the method validity.

Biography

Paolo Neri is an assitant professor at the University of Pisa, Department of Civil and Industrial Engineering, Pisa, Italy. His research activity is focused on experimental dynamic characterization of mechanical components through classical local methods and innovative full-field techniques.

References

1. N. Rieger, The high cost of failure of rotating equipment., in: Proceedings of the 44th Meeting of the Mechanical Failures Prevention Group, 1990, pp. 1–17, aD-A226 670.
2. A. Oberholster, P. Heyns, Online condition monitoring of axial-flow turbomachinery blades using rotor-axial eulerian laser doppler vibrometry, Mechanical Systems and Signal Processing 23 (5) (2009) 1634–1643, doi: 10.1016/j.ymssp.2009.01.001.
3. P. Neri, B. Peeters, Non-harmonic fourier analysis for bladed wheels damage detection, Mechanical Systems and Signal Processing 356 (2015) 181–194.
4. P. Neri, Bladed wheels damage detection through Non-Harmonic Fourier Analysis improved algorithm, Journal of Sound and Vibration 88 (2017) 1–8.
5. R. Bishop, D. Johnson, The Mechanics of Vibration, Cambridge University Press, 1979.
6. H. Bloch, M. Singh, Steam Turbines: design, applications and re-rating, 2nd Edition, McGraw-Hill, 2008.
7. M. Singh, J. Vargo, Reliability Evaluation of Shrouded Blading Using the SAFE Interference Diagram, Journal of Engineering for Gas Turbines and Power 111 (4) (1989) 601–609, doi: 10.1115/1.3240296.
8. M. Singh, B. Thakur, W. Sullivan, G. Donald, Resonance Identification for Impellers, in: Proceedings of the 32nd Turbomachinery Symposium, 2003, pp. 59–70.
9. L. Bertini, P. Neri, C. Santus, A. Guglielmo, G. Mariotti, Analytical investigation of the safe diagram for bladed wheels, numerical and experimental validation, Journal of Sound and Vibration 333 (19) (2014) 4771–4788, DOI: 10.1016/j.jsv.2014.04.061.
10. L. Bertini, B. Monelli, P. Neri, C. Santus, A. Guglielmo, Robot assisted modal analysis on a stationary bladed wheel, in: Proceedings of the ASME 2014 12th Biennial Conference on Engineering Systems Design and Analysis - ESDA, Copenhagen, Denmark, 2014.
11. L. Bertini, P. Neri, C. Santus, A. Guglielmo, Automated Experimental Modal Analysis of Bladed Wheels with an Anthropomorphic Robotic Station, Experimental Mechanics 57 (2) (2017) 273–285, DOI 10.1007/s11340-016-0223-5.
12. L. Bertini, P. Neri, C. Santus, One exciter per sector test bench for bladed wheels harmonic response analysis, in: Proceedings of the Turbo Expo 2017: Turbomachinery Technical Conference and Exposition, Charlotte, NC, USA, 2017.
13. T. Berruti, C. Firrone, M. Gola, Banco sperimentale per la risposta forzata non lineare di dischi palettati con un sistema di eccitazione non a contatto, in: Porceedings of 40 Convegno Nazionale AIAS - Associazione Italiana per l'Analisi delle Sollecitazioni, Palermo, Italy, 2011.
14. C. Firrone, T. Berruti, An electromagnetic system for the non-contact excitation of bladed disks, Experimental Mechanics 52 (2012) 447–459, dOI 10.1007/s11340-011-9504-1.
15. L. Pesek, F. Vanek, V. Bula, J. Cibulka, Excitation of blade vibration under rotation by synchronous electromagnet, Engineering MECHANICS 18 (3/4) (2011) 249–257.
16. C. Firrone, T. Berruti, M. Gola, On force control of an engine order-type excitation applied to a bladed disk with underplatform dampers, Journal of Vibration and Acoustics 135 (2013) 1–9.
17. P. Neri, Excitation device for high frequency vibration analysis: Design and test results, Journal of Vibration and Control (2017) 1–10.
18. G. Battiato, C. M. Firrone, T. Berruti, A benchmark for tip timing measurement of forced response in rotating bladed disks, in: 11th International Conference on Engineering Vibration, Ljubljana, Slovenia, 2015.
19. A. Boczkowska, L. Czechowski, T. Niezgoda, Analysis of magnetic field effect on ferromagnetic spheres embedded in elastomer pattern, Journal of Theoretical and Applied

Mechanics 48 (2010) 659–676.
20. J. Bigegn, J. Sabonnadiere, J. Coulomb, Finite element analysis of an electromagnetic brake, IEEE Transaction on magnetics MAG-19 (6).
21. I. Yatchev, K. Hinov, V. Gueorgiev, 3d finite element modelling of a permanent magnet electromagnetic valve actuator, Annals of the University of Craiova, Electrical Engineering series (32), iSSN 1842-4805.
22. I. Yatchev, N. Ilieva, K. Hinov, 3d finite element modelling of a permanent magnet linear actuator, Serbian Journal of Electrical Engineering 5 (1) (2008) 99–108.
23. L. Ye, D. Li, B. Jiao, Y. Wang, Electromagnetic field analysis in permanent magnet retarder based on finite element method, in: Proceedings of Progress In Electromagnetics Research Symposium, Cambridge, USA, 2010.
24. E. Barzi, G. Gallo, P. Neri, Fem analysis of nb-sn rutherford-type cables, IEEE Transaction on applied supercoductivitty (3).
25. A. Proca, A. Keyhani, A. EL-Antably, W. Lu, M. Dai, Analytical model for permanent magnet motors with surface mounted magnets, IEEE Transaction on energy conversion 18 (3).
26. H. Tiegna, Y. Amara, G. Barakat, Overview of analytical models of permanent magnet electrical machines for analysis and design purposes, Mathematic and Computers in Simulation 90 (2013) 162–177.
27. E. Furlani, Permanent Magnet and Electromechanical Dedvices, Academic Press Series in Electromagnetism, 2001.